


TiO₂ Immobilized on Fibrous Clay as Strategies to Photocatalytic Activity

Wemerson Vieira de Oliveira^a, Alan Ícaro Sousa Morais^a, Luzia Maria Castro Honorio^a,
Pollyana Aragão Trigueiro^a, Luciano Costa Almeida^b, Ramón Raudel Peña Garcia^a,
Bartolomeu Cruz Viana^a, Marcelo B. Furtin^a, Edson Cavalcanti Silva-Filho^a, Josy Anteveli Osajima^{a*} 

^aUniversidade Federal do Piauí (UFPI), Laboratório interdisciplinar de materiais avançados (LIMAV),
Teresina, PI, Brasil

^bUniversidade Federal de Pernambuco (UFPE), Departamento de Engenharia Química (DEQ),
Recife, PE, Brasil

Received: August 12, 2019; Revised: December 02, 2019; Accepted: January 10, 2020

TiO₂ immobilized in Sepiolite (TiO₂/Sep) was successfully prepared by the sol-gel technique, with titanium isopropoxide as the precursor for the formation of TiO₂ in the anatase phase calcined at 400 °C. The prepared samples were characterized by X-ray diffraction, Fourier Transform Infrared spectroscopy, Scanning Electron Microscopy coupled to energy dispersive spectroscopy, and thermogravimetric analysis. The results showed that TiO₂/Sep structure was identified in all characterizations, showing the specific peaks, bands, mass loss, and morphology after the impregnation process. Photocatalytic experiments were performed under UV irradiation with various photocatalyst concentrations and pH effects in the reaction. The prepared samples presented 72% photocatalytic efficiency for eosin (EA) dye discoloration after 150 min under UV light. This efficiency was attributed to the radicals generated from the TiO₂ and the high specific surface area, showing that TiO₂/Sep is promising candidate in the degradation of organic pollutants.

Keywords: *Sepiolite, dye, environmental remediation, discoloration.*

1. Introduction

Among the anthropogenic activities that have contributed to the degradation of water quality, industrial activity is undoubtedly one of the main sources of pollution^{1,2}. Synthetic dyes are extensively used in various textures, in the production of leather, cosmetics, paper, food, and pharmaceuticals, among others³.

Among them, eosin (EA) is an anionic dye (C₂₀H₆Br₄Na₂, 2,4,5,7-tetrabromofluorescein) widely used in dyeing, printing, leather, and fluorescent pigments to offer reddish coloration on wool fabrics^{4,6}. Toxicological information shows that it may cause irritation to the skin and eyes, and ingestion may have several adverse effects on vital organs such as liver and kidneys. Dye inhalation reduces gaseous exchange in the lungs, and its metabolites are highly toxic and carcinogenic^{7,8}.

Ecologically correct and economically viable technologies have guaranteed the quality of the water resources through the degradation or immobilization of these compounds in effluents^{9,10}. Advanced oxidative processes (AOPs) have been especially highlighted for their ability to degrade a large number of recalcitrant substances through procedures that require only simple and low-cost operations^{11,12}. Among photochemical AOPs, photocatalysis is an emerging technology for the degradation of organic pollutants¹³. There are several advantages over competing processes, such as complete mineralization, ambient temperature and pressure conditions,

and, above all, a reduction in environmental impact for solid waste disposal^{13,14,15}.

Based on the photocatalytic scope, the application of clay-based materials as carriers and/or heterostructures with semiconducting oxides¹⁶⁻¹⁹, for example, TiO₂ (titania) has attracted growing interest due to its properties of low toxicity, low cost and high photocatalytic efficiency, are being used as reference and/or standard photocatalysts because they combine attractive properties like chemical stability, high oxidizing power and nontoxicity²⁰⁻²³. However, despite the positive aspects, there are some limitations that hinder its practical application as the low surface area of TiO₂ and extremely thin thickness causing difficulty in the separation, recovery and reuse of particles and/or nanoparticles in aqueous solution^{15,24-26}. Thus, TiO₂ clusters become unfavorable to photocatalytic process²⁷.

Modified clay materials have recently been used in the treatment of various polluting compounds^{3,14,18,28-30} to allow alterations in the semiconductor structure that favor charge separation mobility and, consequently, the yield in a photocatalytic oxidation process¹⁸. In addition, clay minerals are promising candidates for support due to their strong mechanical-chemical stability, cost-effectiveness, good adsorption capacity, which minimizes TiO₂ nanoparticle aggregation, inducing enhanced photocatalytic performance^{15,31,32}.

Researchers have been preparing photocatalysts supported from various types of mineral clay^{15,22,33,34}. For example, Bel Hadjltaief et al.³ used a TiO₂ coated Tunisian clay to remove reactive blue anion 19 (RB19). The degradation

*e-mail: josyosajima@ufpi.edu.br

percentages were 99% and 78%, respectively, after only 90 min of irradiation under UV light and sunlight, indicating the efficiency of TiO₂/clay due to the stability of the anatase phase that simultaneously attacked the RB19 dye.

In particular, sepiolite is a naturally occurring phyllosilicate with a fibrous morphology found in a wide variety of geological environments and has been extracted for centuries because of its useful properties, such as good adsorption capacity and non-toxicity³⁵. In addition, sepiolite is prominent in the photocatalytic field due to its high surface area, around 210 m²/g, which can be used as photocatalytic support and its morphology^{19,36}, composed of molecular-sized structural channels growing in the direction of the fibers^{15,19}. Another relevant characteristic is the acidic centers [SiO₄] in their structure, capable of structurally modifying the compounds and easily to the degradation process^{15,19,37}.

In relation to photocatalysis and the use of sepiolite, Liu et al.²¹, synthesized a new composite called AgTiS (Ag+TiO₂+sepiolite) and systematically studied, under UV and visible light, methyl orange degradation. According to the results, TiO₂, Sep, TiO₂/Sep, and AgTiS showed higher photocatalytic activity due to several factors, such as the band gap energy, charge separation, pore distribution, and higher adsorption capacity. In this same sense, Zhou et al.¹⁵ evaluated the degradation of the orange G dye using nanocomposites of the TiO₂ and Sep.

In this sense, this work uses a kind of derived-clay material to evaluate the photocatalytic oxidation process of eosin y anion dye under UV irradiation. TiO₂ was immobilized onto fibrous support and has been used for synthesize TiO₂/Sep functional material for application as a photocatalyst.

2. Materials and Methods

2.1 Chemicals, treatment of clay and immobilization of sepiolite (TiO₂/Sep)

Sepiolite (Sep) was donated by Tolsa (Spain). The reagents and materials used were titanium isopropoxide IV [Ti(OCH(CH₃)₂)₄], analytical grade 97% (Sigma-Aldrich); hydrogen peroxide (H₂O₂, 35%, 130 volume) (Anidrol); ethyl alcohol (C₂H₆O) P.A 99.5% (Dinâmica), titanium dioxide (Vetec), and organic yellow eosin dye (C₂₀H₆Br₄Na₂O₅), 691.86 g mol⁻¹ (Dinâmica) (EA).

In the synthesis, sepiolite (Mg₈Si₁₂O₃₀(OH)₄(OH₂)₄·nH₂O; n ≤ 8) was deagglomerated and underwent treatment for removing impurities and organic matter, as described by Almeida et al.³⁸. The immobilization of titanium dioxide in the clay was carried out by the sol-gel method. For the synthesis, 6.0 mL (0.02 mol) of titanium isopropoxide Ti(OCH(CH₃)₂)₄ and 6.0 mL (0.33 mol) of H₂O were mixed and then diluted in 100.0 mL (1.72 mol) of ethyl alcohol (C₂H₆O), to obtain the sol phase. Then the mixture was magnetically stirred for 1 h. In another beaker, 5.0 g sepiolite and 20.0 mL of ethanol were mixed and magnetically stirred for 30 min. The two solutions were then mixed in a single vessel and allowed to stand for 24 h. After this process, the obtained material was dried at 75°C for 12 h in an oven, deagglomerated and calcined in a muffle furnace at 400°C for 2 h with a heating rate of 10 °C min⁻¹. The obtained material was stored and

represented by TiO₂/Sep. The TiO₂/Sep ratio was 1:5 (m/m), considering the amount used in the synthesis.

2.2 Photocatalytic activity

The photocatalytic activity tests were performed in a photochemical reactor containing 180.0 mL of dye solution under magnetic stirring at 700 rpm. This reactor was coupled to a thermostatic bath (TECNAL-TE-2005) at 25.0 ± 1.0 °C. The radiation source used was a 125 W mercury without bulb³⁹, which intensity was monitored using a radiometer (HANNA - HI 97500, Luxmeter), obtaining a value of 10.00 ± 1.00 μW cm⁻¹. Samples were withdrawn at time intervals of 0, 5, 10, 15, 30, 45, 60, 90, 120 and 150 minutes of irradiation. The discoloration activity was monitored using a CARY 300 model UV-Vis spectrophotometer in the 200–800 nm range. The photocatalytic tests were performed with 0.5, 1.0, and 1.5 g L⁻¹ of the catalyst. Changes in the EA concentration were monitored at 516 nm, the maximum wavelength region of the dye⁷. Also, the effect of pH on the degradation of the dye at 2.0x10⁻⁵ mol/L was tested at three distinct pH values (4.0, 7.0 and 10.0) by the addition of NaOH and/or HCl.

2.3 Characterization

The Sepiolite and TiO₂/Sep were characterized by X-ray diffraction (XRD), with Cu-Kα radiation (λ = 1.5406Å). The tests were done with an angular range of 3–75° (2θ) and a sweep rate of 2° min⁻¹ in continuous mode. Fourier transform infrared spectroscopy (FTIR) (Bruker VERTEX 70) in transmittance mode, in the 4000–400 cm⁻¹ region, 64 scans and 4 cm⁻¹ resolution was carried out on the powders. The textural properties of the solids were investigated by adsorption-desorption analysis of N₂ at 77 K using Quantachrome Autosorb-iQ Instruments. Thus, before each analysis, about 200 mg of the sample was degassed for 4 hours at 200 °C. The surface area was calculated by the Brunauer-Emmett-Teller (BET) method and to estimate the volume and pore diameter the Barrett-Joyner-Halenda (BJH) method was used from the N₂ adsorption curves. Thermal stability analysis of the clay and compound was performed on a TA Instruments model SDT Q600. Between 5.0 and 7.0 mg of sample were used for the tests. The materials were heated at 10 °C min⁻¹ to 900 °C under a 50 mL min⁻¹ argon flow. Morphological analysis was performed using coupled scanning electron microscopy-dispersive energy spectroscopy (SEM-EDS); the tests were carried out on a field-emitting electron-emitting device (SEM-FEI, FEG-250).

3. Results and Discussion

3.1 Characterization

The XRD diffractograms of sepiolite (a) and TiO₂/Sep (b) are presented in Figure 1. The sepiolite showed reflections on 2θ = 7.44°, 12.06°, 13.38°, 17.86°, 19.90°, 20.76°, 23.72°, 26.74°, 28.12°, 35.16°, 36.84°, and 40.14°, attributed to the (110), (130), (200), (150), (060), (131), (260), (400), (331), (191), (291), and (541) planes; indexing of the planes was done according to reference crystallographic sheet JCPDS 75-1597^{40,41}. For the immobilized system, new peaks appeared

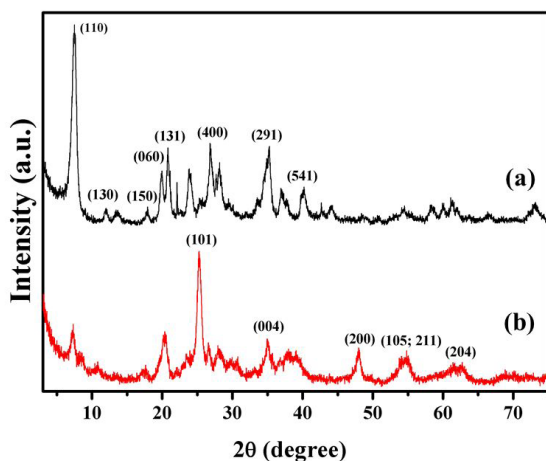


Figure 1. X-ray diffractograms of Sepiolite (a) and TiO₂/Sep nanocomposite (b).

with reflections around $2\theta = 25.26^\circ, 37.96^\circ, 48.00^\circ, 54.06^\circ, 54.96^\circ,$ and 62.74° , which correspond to the (101), (004), (200), (105), (211), and (204) planes typical of TiO₂ in the anatase phase⁴²⁻⁴⁴. The most intense and characteristic diffraction peak of TiO₂ in the anatase phase was detected at 25.30° and was attributed to the (101) plane. As can be seen from the plane overlays, the crystallinity of clay decreased compared to the material with TiO₂ immobilized, although it maintains the crystallographic profile of the sepiolite, ensuring incorporation of the oxide into the clay structure, as identified by the XRD technique.

Figure 2 presents the FTIR of sepiolite and TiO₂/Sep. The bands between 3700 and 3400 cm⁻¹ are attributed to the presence of different types of hydroxyl presented in the water molecules of mineral structure (adsorbed and zeolite water) and to the OH group octahedral coordinated with Mg and the surface. The bands between 3700 and 3570 cm⁻¹ correspond to the vibration elongation of hydroxyl groups (OH) attached to the octahedral sheet with Mg ions located in the channels of the sepiolite and to elongation vibrations at the clay surface. A characteristic band at 3574 cm⁻¹ is attributed to water-coordinated Mg (Mg-OH stretching vibration)^{36,40,45}. The OH group at around 1669 cm⁻¹ refers to the presence of zeolite water in the nanostructured channels of the clay. The bands at 690 cm⁻¹ and 440 cm⁻¹ are respectively attributed to the presence of hydroxyl (OH) group elongation vibrations bound to the octahedral sheet with magnesium ions and the vibrations of Si-O-Mg bonds. Bands between 1031 and 1400 cm⁻¹ are characteristic of silicates and appear due to the vibration of Si-O-Si bonds^{40,45}.

When comparing the sepiolite and TiO₂/Sep spectra, bands appear at 3421 and 1639 cm⁻¹, promoted by stretching vibrations through the interaction of water molecules on the surface of the oxide. The disappearance of the bands at 3618 and 3557 cm⁻¹ can be explained by the immobilization of the TiO₂ particles in the clay by condensation of the hydroxyl groups of the titanium precursor with the hydroxyls of the clay occurring during thermal treatment at 400°C, corroborating with Zhang et al.³⁶.

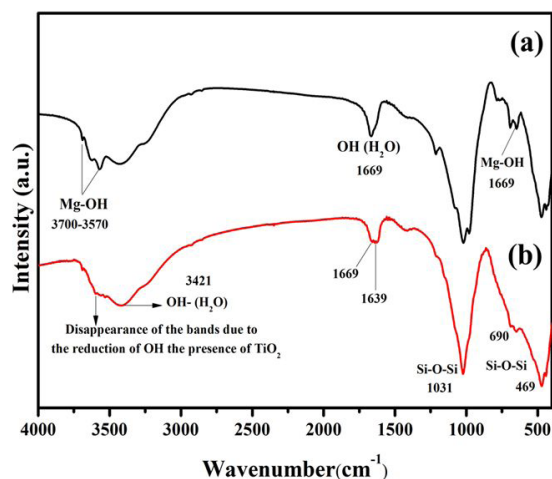


Figure 2. Infrared spectra for Sepiolite (a) and TiO₂/Sep composite (b).

The N₂ gas adsorption and desorption isotherms of the Sep and TiO₂/Sep samples at 77K are shown in Figure 3, where P/P₀ represents the relative vapor pressure of N₂ and V is the adsorbed/desorbed N₂ volume (Figure 3).

It is observed that the isotherms for both materials exhibit similar behavior. According to the classification determined by the *International Union of Pure and Applied Chemistry* (IUPAC), the materials presented type IV isotherms, which are defined as mesoporous materials (corroborating the pore distribution, with pore diameter from 2 to 50 nm). A small amount of macropores can also be attributed to the porosity generated by intraparticle grains⁴⁶. Besides, it was observed a deviation in the desorption curves, which is called hysteresis, a phenomenon caused by capillary condensation. This hysteresis consists of the phase shift of N₂ (from gas to liquid phase) within the pore at a pressure lower than its saturation pressure, caused by the formation of concave shaped meniscus in a group of pores of specific size and shape⁴⁷. According to the IUPAC classification, the hysteresis demonstrated by the materials is represented by type H₃⁴⁸. This type of hysteresis can be attributed to materials having interleaved layer aggregates that give rise to slit-shaped pores.

The surface area, the pore volume and their diameter were calculated from the obtained isotherms and the application of the BET and BJH methods as shown in Table 1.

After incorporation of the oxide into the clay structure, the average pore diameter decreased and the specific area decreased⁴⁹, probably due to a significant decrease in the mesoporous area due to the introduction of the oxide and a slight increase in the amount of pore micropores in the region near 2 nm due to the TiO₂ formed.

Figure 4 shows the thermogravimetric (TG) and derivative (DTG) curves, which show the mass loss events for sepiolite and TiO₂/Sep nanocomposite during four different events⁴⁵. For pristine sepiolite, the first event, at approximately 63 °C, comes from the dehydration of surface water and the zeolitic water in the channels, with 5.4% mass loss. At approximately 264 °C there is a second event corresponding to the departure of water molecules coordinated to the Mg atoms of the

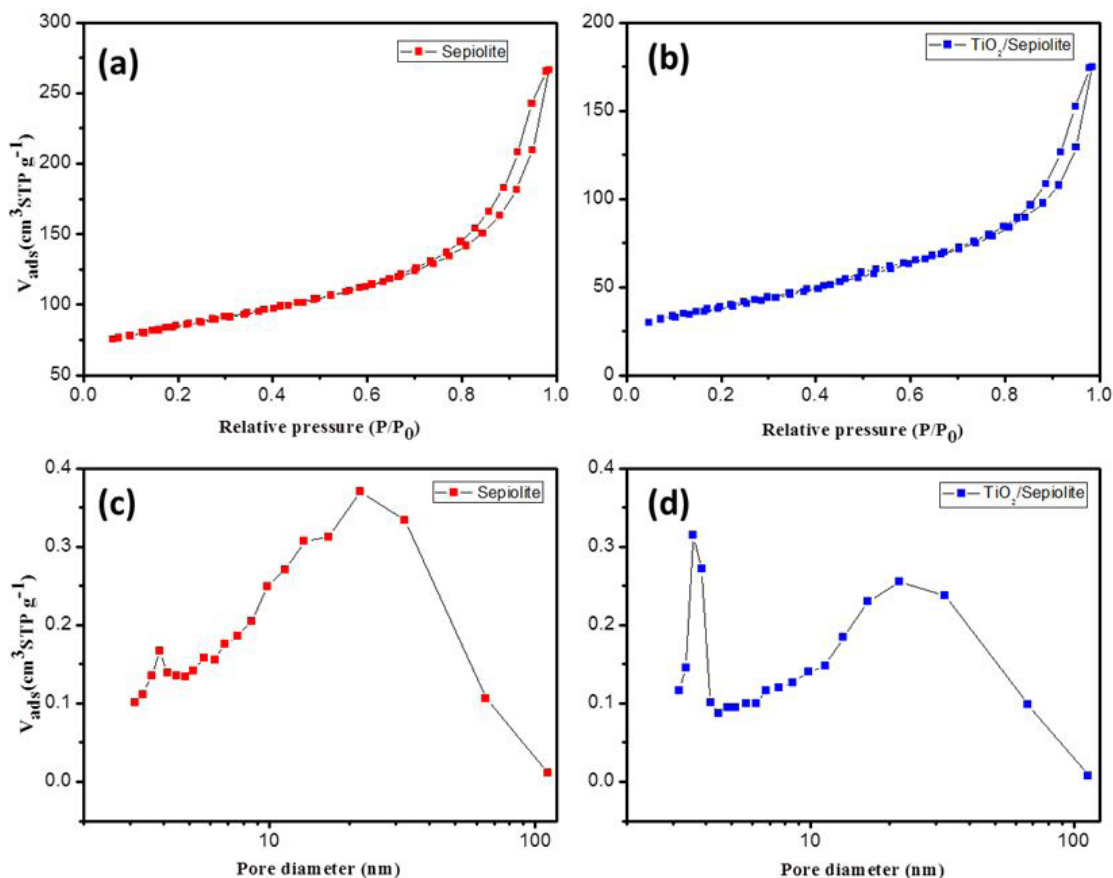


Figure 3. Adsorption/desorption isotherms at (a) sepiolite clay mineral, (b) TiO_2/Sep catalyst and size pore distribution at (c) sepiolite and (d) TiO_2/Sep .

Table 1. Specific surface area, pore volume and mean pore diameter values.

	A_{BET} ($\text{m}^2 \text{g}^{-1}$)	Vp ($\text{cm}^3 \text{g}^{-1}$)	Mean pore diameter (nm)
Sepiolite	277.9	0.32	3.86
TiO_2/Sep	137.0	0.24	3.58

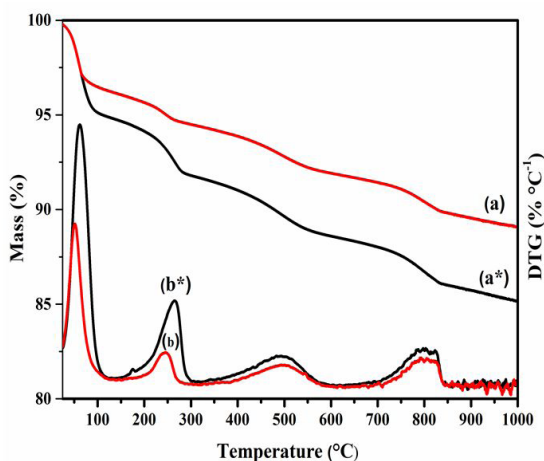
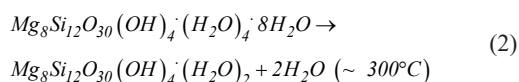
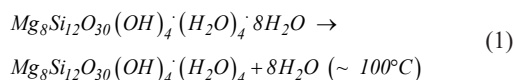
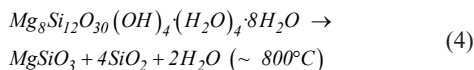
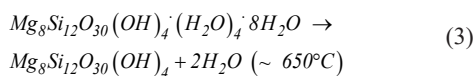


Figure 4. TG curves of sepiolite clay (a^*) and TiO_2/Sep nanocomposite (a) and DTG curves of sepiolite clay (b^*) and TiO_2/Sep nanocomposite (b).

octahedral sheet, with a 3.0% mass loss. The third event occurs between 400 and 600 °C is attributed to the departure of the second coordinating water molecule, with a mass loss of around 2.8%. At 800 °C, a fourth event is observed, with a 2.2% mass loss that is attributed to dehydroxylation of the octahedrally coordinated hydroxyl groups. As a result of dehydroxylation, the so-called anhydrous sepiolite is transformed into an amorphous phase called meta-sepiolite. Mass losses above 800°C are due to total dehydroxylation of the clay structure and formation of the enstatite phase (MgSiO_3)⁵⁰. According to Perraki and Orfanoudaki⁴⁵, the transformations occurring are represented by the chemical reactions (1-4):





Despite the similarity between the thermogravimetric curves of sepiolite and TiO₂/Sep, less significant mass losses were observed in the nanocomposite, thus evidencing alterations in the composition of the material after incorporation of the oxide. The main differences between the compounds occur in the first two events since, after the incorporation of TiO₂, the hydroxyl groups were reduced due to the condensation of these groups in the immobilization process⁴⁴. Zeolite water loss was observed at 52 °C, with a 2.8% mass loss. Co-ordinated water removal from TiO₂ was observed at approximately 245 °C with approximately 1.2% mass loss. The species chemically adsorbed in the sepiolite structure had a maximum degradation temperature of approximately 500 °C and a 2.1% loss of mass. Finally, dehydroxylation of the nanocomposite was observed with a maximum temperature of 800 °C and a 1.7% mass loss.

3.2 SEM analysis

The SEM image for sepiolite shows the aggregation of microfibrils that can have sizes up to 100 nm and have a large specific surface area⁵¹. Analyzing the SEM image present in Figure 5a, the sepiolite presents a fibrous morphology. The immobilized material (Figure 5b, c) is observed along with fibrous morphology and the formation of agglomerates in a rounded form, which reinforces the presence of TiO₂ in the anatase form incorporated into the surface of the clay⁵¹. In addition, the presence of the constituent elements of sepiolite, silicon, oxygen and, magnesium, were observed along with small amounts of aluminum and iron in the SEM-EDS analyses (Figure 6). This observation was also made by Bahabadi et al.⁵², showing the main constituent of sepiolite and the secondary elements highlighted in this work. The EDS spectrum for the TiO₂/Sep material identified the presence of all the mentioned elements, in addition to titanium after chemical modification⁴¹.

For a better understanding of the immobilization of the oxide in the clay network, the formation of the TiO₂ oxide can be expressed using small colloidal Ti(OH)₄ particles that precipitate on the surface of the sepiolite and interact with the surface hydroxyls of fibers, thus generating the incorporated TiO₂ particles. A possible formation mechanism for this particle process is suggested schematically in Figure 7.

3.3 Photocatalytic discoloration of eosin y

The ideal concentration of photocatalyst is one of the main factors that affect the efficacy and rate of a photocatalytic reaction since it directly interferes in the rate of degradation reaching a critical yield value⁵³⁻⁵⁷. Preliminarily, photocatalytic tests were performed against EA discoloration (2.0x10⁻⁵ mol L⁻¹) in aqueous solution, in order to effectively verify whether the textile compound is degraded. Photolytic and photocatalytic quantifications were monitored by the decrease of the characteristic peak at 516 nm, the maximum wavelength of

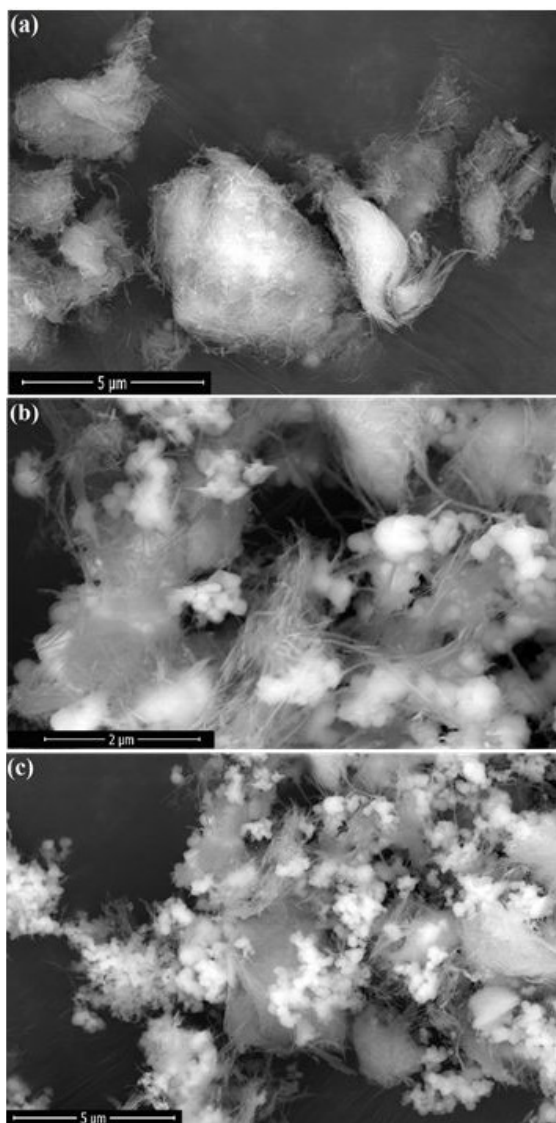


Figure 5. SEM images for Sepiolite (a) and TiO₂/Sep composite (b-c).

the chromophore groups. Figure 8 shows the UV-Vis spectra for TiO₂/Sep catalyzed dye discoloration at concentrations of 0.5, 1.0 and 1.5 g L⁻¹ and the respective degradation percentages. According to the discoloration process, EA was photocatalytically oxidized at all concentrations, although the 1.0 g L⁻¹ (0.18 g to 180 mL) showed a higher discoloration rate. It is known that excess photocatalyst may cause a reduction in radiation passage due to particle aggregation and/or solution turbidity^{27,58-60} compromising the passage of light and reducing discoloration. As this condition was compromised, the maximum concentration of photocatalyst guaranteed an oxidation yield lower than the intermediate variation studied. In addition, it is possible to observe, from the economic point of view, that when incorporating TiO₂ in the clay structure to obtain TiO₂/Sep, the conversion reaches about 72% in 150 min of reaction, thus obtaining a 2.5 times increase than Sep (Figure 9). Specifically, clays of this type have a shielding effect; that is, they can absorb

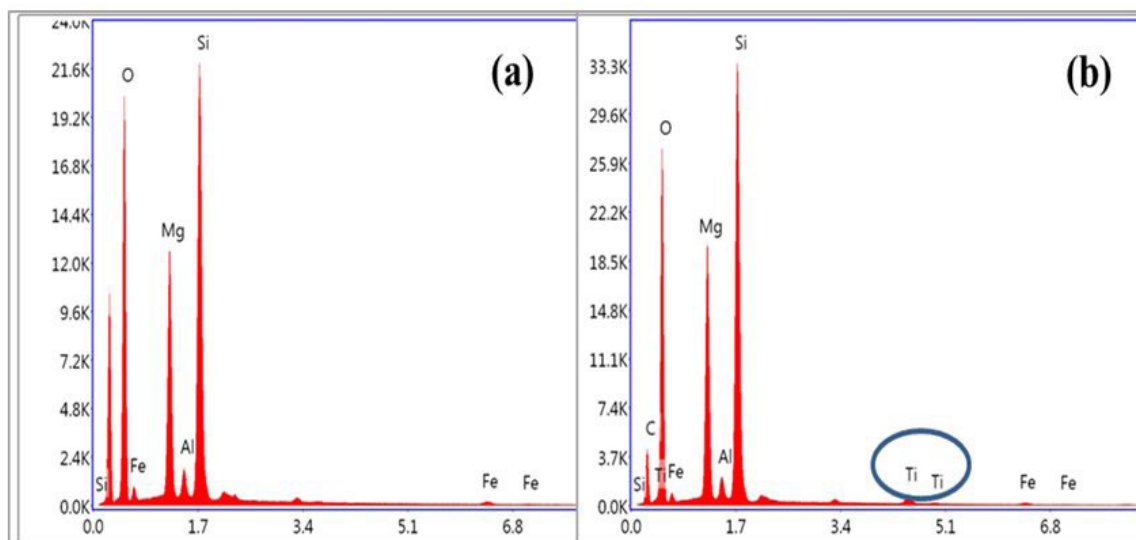


Figure 6. EDS spectrum of Sepiolite (a) and TiO₂/Sep composite (b).

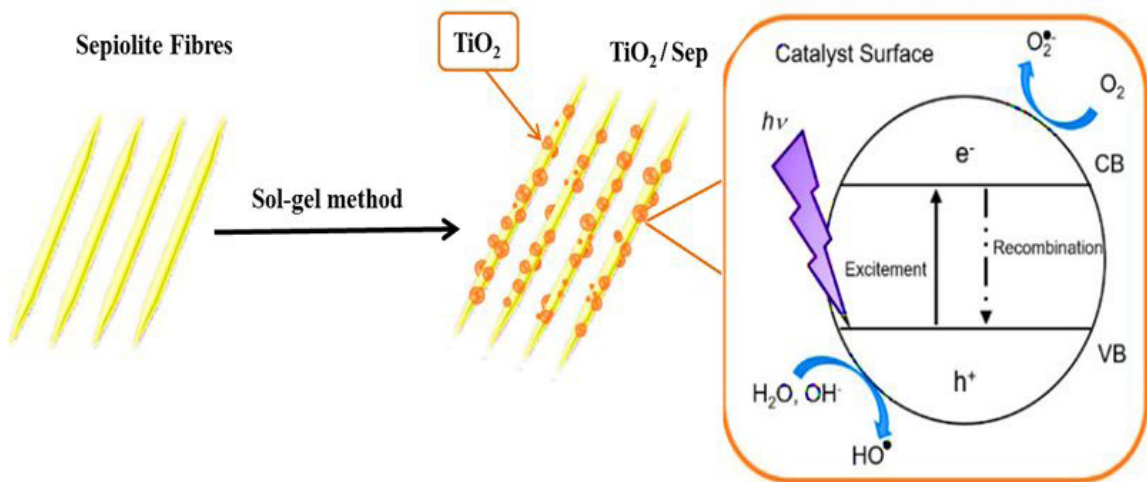


Figure 7. Schematic diagram of the immobilization of TiO₂ to the sepiolite surface and of a possible photodegradation mechanism of eosin y dye over TiO₂/Sep photocatalyst.

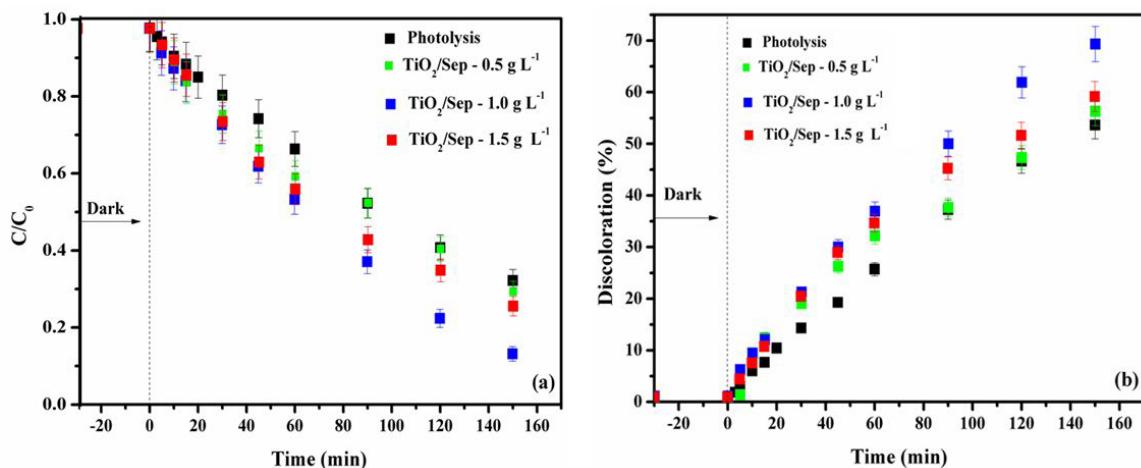


Figure 8. Variation of EA absorption at different concentrations of TiO₂/Sep (a), discoloration rates of EA dye as a function of irradiation time (b).

or disperse incoming UV light, causing a reduction of the photocatalytic process. Thus, Sep behaves as a blocker in the dye degradation process⁶¹.

The main reason for the high activity of TiO₂/Sep is probably due to the structural modifications caused by the oxide that act to favor charges separation mobility in the interstitial interior to favor the oxidation process and avoid recombination between the oxide loads and clay^{14,18}. Another important factor in efficient activity may be the high surface area of the composite, resulting from the synergistic effect between TiO₂ and clay³⁶. Besides, the pristine TiO₂ showed a 68% discoloration of the dye in the same condition, showing that the composite is better than pristine materials (sepiolite and TiO₂). It is also believed that the ratio of TiO₂:Sep (w/w) used to obtain the desired phase was essentially important for generating highly oxidizing radicals (OH, O₂^{•-}) since TiO₂ is able to oxidize organic compounds due to its electronic properties and bandgap value suitable to the region of UV light¹⁴. This efficiency was

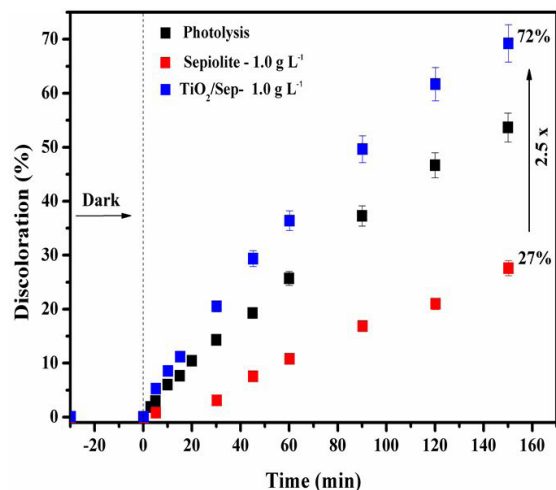
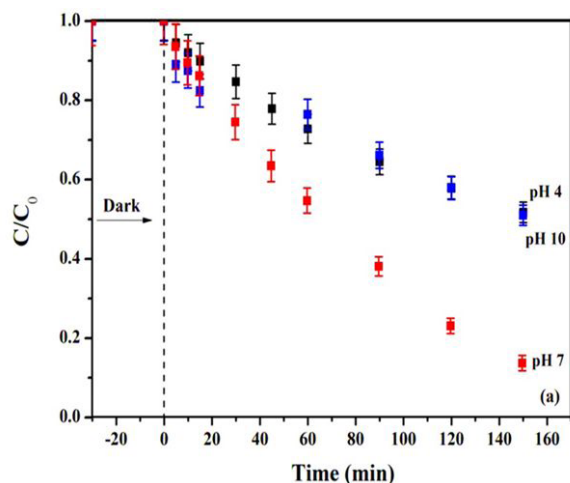
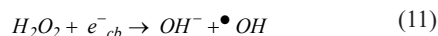
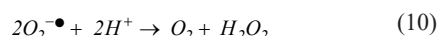
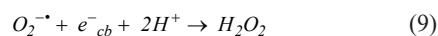
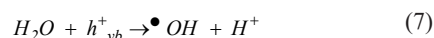
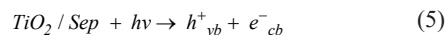


Figure 9. Discoloration rates of the EA dye at the optimum concentration (1.0 g L⁻¹) as a function of the irradiation time of 150 min.



also observed by Zhang et al.³⁶ using TiO₂/Sep composites, prepared at low temperature by the sol-gel technique, in the degradation of red acid G (ARG) and 4-nitrophenol (4-NP). The results obtained showed that 99.2% of ARG was degraded after 120 min, whereas 4-NP (hardly degradable pollutant) reached 79% conversion after 240 min. The results suggested that the TiO₂/Sep composite is a promising candidate for degrading pollutants under UV illumination.

In general, during the photocatalytic process, species formed by the action of the photocatalyst favor the degradation process represented by the following Equations 5-12⁶⁰:



Another important factor is the pH of the solution⁶². The concentration variations and discoloration percentages (Figure 10) showed that the higher photocatalytic performance of the TiO₂/Sep material was at neutral pH. The pH variation changes the surface charge of the TiO₂ particles, in other words, under acid or alkaline conditions the TiO₂ surface can be protonated or deprotonated, according to Equations 13 and 14, respectively⁶⁰.

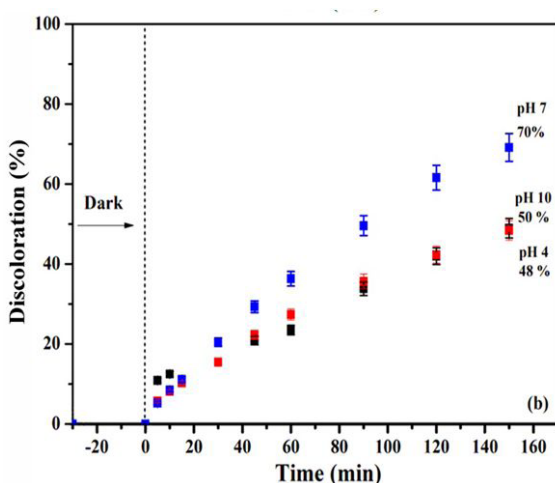
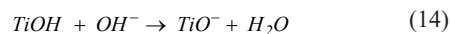
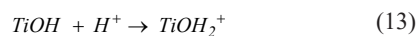


Figure 10. Effect of pH on EA discoloration using TiO₂/Sep (a), rate of EA dye discoloration as a function of irradiation time (b).

Thus, the surface of TiO₂ present in the material will remain positively charged in acid media and negatively charged in basic media. According to the literature⁵⁴, TiO₂ has higher oxidizing activity at acidic pH, although excess H⁺ ions can decrease the reaction rate. The fact that the pH test has the best efficiency at neutral pH can be explained by the fact that hydroxyl radicals are considered the predominant species at neutral and basic pH. These •OH radicals are easier to generate by oxidation with more hydroxyl ions available on the TiO₂ surface, causing process efficiency to increase. In contrast, excess OH⁻ ions hinder the formation of hydroxyl radicals at basic pH. It is also worth noting that in alkaline solutions there will be coulombic repulsion between the negatively charged surface of the photocatalyst and the hydroxide anions, which could prevent the formation of •OH and thus decrease the photo-oxidation to promote competition between the anionic charges of the dye and the surface of the photocatalyst^{60,63}. With excess •OH there will also be competition between molecules of the anionic dye to adsorb on the surface of the photocatalyst⁶³. Therefore, the nature of the dye (anionic or cationic), surface, and pH are factors that directly influence the activity of the photocatalyst.

4. Conclusions

In the present work, TiO₂/Sep samples were successfully obtained by the sol-gel method at 400°C. The presence of TiO₂ nanoparticles in the clay structure decreased the crystallinity of Sepiolite. The infrared results showed the characteristic spectra of the sepiolite clay and some alterations upon the immobilization and interaction of the TiO₂ with the clay, such as the disappearance of the band at 3700 cm⁻¹ and the appearance of a new band around 1669 cm⁻¹. Through scanning electron microscopy, the presence of clay fibers and agglomerated spherical particles of TiO₂ was observed in the nanocomposite as well as the presence of the constituent elements of clay and TiO₂. The photocatalytic results showed that at a 1.0 g L⁻¹ concentration had a higher EA discoloration rate (72% in 150 min). This improved performance for TiO₂/Sep system can be attributed to the synergy of the isolated systems (TiO₂+clay) associated with the formation of intermediate energy bands that suppress electron/hole recombination and consequently lead to the generation of oxidative species and final dye conversion. Another important factor in efficient activity may be the composite's high surface area resulting from the synergistic effect between TiO₂ and clay. Finally, the importance of optimizing operational parameters to guarantee success and cost/benefit for future applications in photocatalytic processes for the degradation of emerging pollutants.

5. Acknowledgements

The authors are indebted to CNPq and CAPES for financial support and for fellowships, and to the Interdisciplinary Laboratory of Advanced Materials- LIMAV, Piauí, Brazil.

6. References

- Mahmoud A, Freire RS. New methods for enhancing ozone efficiency on contaminated water treatment. *Quim Nova*. 2007;30:198-205.
- Lee SS, Bai H, Liu Z, Sun DD. Green approach for photocatalytic Cu(II)-EDTA degradation over TiO₂: toward environmental sustainability. *Environ Sci Technol*. 2015;49(4):2541-8.
- Bel Hadjltaief H, Galvez ME, Ben Zina M, Da Costa P. TiO₂/clay as a heterogeneous catalyst in photocatalytic/ photochemical oxidation of anionic reactive blue 19. *Arab J Chem*. 2019;12(7):1454-62.
- Anitha KSKT, Senthil Kumar P. Synthesis of nano-sized chitosan blended polyvinyl alcohol for the removal of Eosin Yellow dye from aqueous solution. *J Water Process Eng*. 2016;13:127-36.
- Anirudhan TS, Rejeena SR. Photocatalytic degradation of eosin yellow using poly(pyrrole-co-aniline)-Coated TiO₂/nanocellulose composite under solar light irradiation. *J Mater*. 2015;2015:1-11.
- Muhammad MT, Nasiruddin Khan M. Oppositely charged dye surfactant interactions: extent and selectivity of ion pair formation. *J Mol Liq*. 2018;266:591-6.
- Mittal A, Jhare D, Mittal J. Adsorption of hazardous dye Eosin Yellow from aqueous solution onto waste material De-oiled Soya: isotherm, kinetics and bulk removal. *J Mol Liq*. 2013;179:133-40.
- Sharma AK, Priya BS, Kaith BS, Panchal S, Bhatia JK, Bajaj S, et al. Response surface methodology directed synthesis of luminescent nanocomposite hydrogel for trapping anionic dyes. *J Environ Manage*. 2019;231:380-90.
- Araújo KS, Antonelli R, Gaydeczka B, Granato AC, Malpass GRP. Advanced oxidation processes: a review regarding the fundamentals and applications in wastewater treatment and industrial wastewater. *Rev Ambient Água*. 2016;11(2):387-401.
- Moreira FC, Boaventura RAR, Brillas E, Vilar VJP. Electrochemical advanced oxidation processes: a review on their application to synthetic and real wastewaters. *Appl Catal B*. 2017;202:217-61.
- Pétrier C. The use of power ultrasound for water treatment. In: Gallego-Juárez JA, Graff KF, editors. *Power ultrasonics*. Cambridge: Elsevier; 2015, pp. 939-72.
- Han Z, Li J, Han X, Ji X, Zhao X. A comparative study of iron-based PAN fibrous catalysts for peroxymonosulfate activation in decomposing organic contaminants. *Chem Eng J*. 2019;358:176-87.
- Guimarães JR, Guedes Maniero M, Nogueira de Araújo R. A comparative study on the degradation of RB-19 dye in an aqueous medium by advanced oxidation processes. *J Environ Manage*. 2012;110:33-9.
- Belver C, Bedia J, Rodriguez JJ. Titania-clay heterostructures with solar photocatalytic applications. *Appl Catal B*. 2015;176-177:278-87.
- Zhou F, Yan C, Liang T, Sun Q, Wang H. Photocatalytic degradation of Orange G using sepiolite-TiO₂ nanocomposites: optimization of physicochemical parameters and kinetics studies. *Chem Eng Sci*. 2018;183:231-9.
- Szczepanik B. Photocatalytic degradation of organic contaminants over clay-TiO₂ nanocomposites: a review. *Appl Clay Sci*. 2017;141:227-39.
- Mishra A, Mehta A, Basu S. Clay supported TiO₂ nanoparticles for photocatalytic degradation of environmental pollutants: a review. *J Environ Chem Eng*. 2018;6(5):6088-107.
- Belver C, Bedia J, Álvarez-Montero MA, Rodriguez JJ. Solar photocatalytic purification of water with Ce-doped TiO₂/clay heterostructures. *Catal Today*. 2016;266:36-45.
- Zhou F, Yan C, Sun Q, Komarneni S. TiO₂/Sepiolite nanocomposites doped with rare earth ions: preparation, characterization and visible light photocatalytic activity. *Microporous Mesoporous Mater*. 2019;274:25-32.
- Liu B, Yang J, Wang J, Zhao X, Nakata K. High sub-band gap response of TiO₂ nanorod arrays for visible photoelectrochemical water oxidation. *Appl Surf Sci*. 2019;465:192-200.

21. Liu R, Ji Z, Wang J, Zhang J. Solvothermal synthesized Ag-decorated TiO₂/sepiolite composite with enhanced UV-vis and visible light photocatalytic activity'. *Microporous Mesoporous Mater.* 2018;266:268-75.
22. Papoulis D, Panagiotaras D, Tsigrou P, Christoforidis KC, Petit C, Apostolopoulou A, et al. Halloysite and sepiolite -TiO₂ nanocomposites: synthesis characterization and photocatalytic activity in three aquatic wastes. *Mater Sci Semicond Process.* 2018;85:1-8.
23. Stathatos E, Papoulis D, Aggelopoulos CA, Panagiotaras D, Nikolopoulou A. TiO₂/palygorskite composite nanocrystalline films prepared by surfactant templating route: synergistic effect to the photocatalytic degradation of an azo-dye in water. *J Hazard Mater.* 2012;211-212:68-76.
24. Grabowska E. Selected perovskite oxides: characterization, preparation and photocatalytic properties: a review. *Appl Catal B.* 2016;186:97-126.
25. Song S, Xu L, He Z, Ying H, Chen J, Xiao X, et al. Photocatalytic degradation of C.I. Direct Red 23 in aqueous solutions under UV irradiation using SrTiO₃/CeO₂ composite as the catalyst. *J Hazard Mater.* 2008;152(3):1301-8.
26. Inamuddin. Inamuddin. Xanthan gum/titanium dioxide nanocomposite for photocatalytic degradation of methyl orange dye. *Int J Biol Macromol.* 2019;121:1046-53.
27. Papoulis D, Komarneni S, Nikolopoulou A, Tsolis-Katagas P, Panagiotaras D, Kacandes HG, et al. Palygorskite- and Halloysite-TiO₂ nanocomposites: synthesis and photocatalytic activity. *Appl Clay Sci.* 2010;50(1):118-24.
28. Fatimah I, Wijaya K, Narsito. Microwave assisted preparation of TiO₂/Al-pillared saponite for photocatalytic phenol photo-oxidation in aqueous solution. *Arab J Chem.* 2015;8(2):228-32.
29. Abdennouri M, Baàlala M, Galadi A, El Makhfouk M, Bensitel M, Nohair K, et al. Photocatalytic degradation of pesticides by titanium dioxide and titanium pillared purified clays. *Arab J Chem.* 2016;9:S313-8.
30. Shao J, Sheng W, Wang M, Li S, Chen J, Zhang Y, et al. In situ synthesis of carbon-doped TiO₂ single-crystal nanorods with a remarkably photocatalytic efficiency. *Appl Catal B.* 2017;209:311-9.
31. Chen D, Zhu Q, Zhou F, Deng X, Li F. Synthesis and photocatalytic performances of the TiO₂ pillared montmorillonite. *J Hazard Mater.* 2012;235-236:186-93.
32. Ökte AN, Tuncel D, Pekcan AH, Özden T. Characteristics of iron-loaded TiO₂-supported montmorillonite catalysts: β -Naphthol degradation under UV-A irradiation. *J Chem Technol Biotechnol.* 2014;89(8):1155-67.
33. Manova E, Aranda P, Angeles Martín-Luengo M, Letaief S, Ruiz-Hitzky E. New titania-clay nanostructured porous materials. *Microporous Mesoporous Mater.* 2010;131(1-3):252-60.
34. Du Y, Tang D, Zhang G, Wu X. Facile synthesis of Ag₂O-TiO₂/sepiolite composites with enhanced visible-light photocatalytic properties. *Chin J Catal.* 2015;36(12):2219-28.
35. Giustetto R, Wahyudi O, Corazzari I, Turci F. Chemical stability and dehydration behavior of a sepiolite/indigo Maya Blue pigment. *Appl Clay Sci.* 2011;52(1-2):41-50.
36. Zhang Y, Wang D, Zhang G. Photocatalytic degradation of organic contaminants by TiO₂/sepiolite composites prepared at low temperature. *Chem Eng J.* 2011;173(1):1-10.
37. Álvarez A, Santarén J, Esteban-Cubillo A, Aparicio P. Current industrial applications of palygorskite and sepiolite. *Developments in Clay Science.* 2011;3:281-98.
38. Almeida LR, Souza JSN, Silva EC Fo, Osajima JA. Attapulgite performance in the degradation of the yellow bright dye. *Mater Sci Forum.* 2016;869:761-4. <http://dx.doi.org/10.4028/www.scientific.net/MSF.869.761>.
39. Araújo FP, Osajima JA, Araújo MRS, Silva EC Fo, Souza JSN. Degradation of colored polystyrene films. *Mater Sci Forum.* 2018;930:254-7. <http://dx.doi.org/10.4028/www.scientific.net/MSF.930.254>.
40. Ma Y, Wu X, Zhang G. Core-shell Ag@Pt nanoparticles supported on sepiolite nanofibers for the catalytic reduction of nitrophenols in water: enhanced catalytic performance and DFT study. *Appl Catal B.* 2017;205:262-70.
41. Fernandes FM, Manjubala I, Ruiz-Hitzky E. Gelatin renaturation and the interfacial role of fillers in bionanocomposites. *Phys Chem Chem Phys.* 2011;13(11):4901-10.
42. Araujo-Lopez E, Varilla LA, Seriani N, Montoya JA. TiO₂ anatase's bulk and (001) surface, structural and electronic properties: a DFT study on the importance of Hubbard and van der Waals contributions. *Surf Sci.* 2016;653:187-96.
43. Anandgaonker P, Kulkarni G, Gaikwad S, Rajbhoy A. Synthesis of TiO₂ nanoparticles by electrochemical method and their antibacterial application. *Arab J Chem.* 2019;12(8):1815-22.
44. Ökte AN, Sayınsöz E. Characterization and photocatalytic activity of TiO₂ supported sepiolite catalysts. *Separ Purif Tech.* 2008;62(3):535-60.
45. Perraki T, Orfanoudaki A. Study of raw and thermally treated sepiolite from the Mantoudi area, Euboea, Greece. *J Therm Anal Calorim.* 2008;91(2):589-93.
46. Zhang Y, Gan H, Zhang G. A novel mixed-phase TiO₂/kaolinite composites and their photocatalytic activity for degradation of organic contaminants. *Chem Eng J.* 2011;172(2-3):936-43.
47. Ertl G, Knözinger H, Schüth F, Weitkamp J. Handbook of heterogeneous catalysts. Weinheim: Wiley-VCH; 2008. <http://dx.doi.org/10.1002/9783527610044>.
48. Lopes JS, Rodrigues WV, Oliveira VV, Braga ANS, da Silva RT, França AAC, et al. Modification of kaolinite from Pará/Brazil region applied in the anionic dye photocatalytic discoloration. *Appl Clay Sci.* 2019;168:295-303.
49. Khumchoo N, Khaorapong N, Ogawa M. Formation of zinc oxide particles in cetyltrimethylammonium-smectites. *Appl Clay Sci.* 2015;105-106:236-42.
50. Zhang Y, Yang Y, Tang K. Physicochemical characterization and antioxidant activity of quercetin-loaded chitosan nanoparticles. *Polym Polymer Compos.* 2007;21:449-56.
51. Vargas Urbano C, Andrea M, Muñoz O, Halil Y, Fernández O, Páez R, et al. Nanoparticles of TiO₂, anatase phase, synthesized by chemical methods. *Ing. y Desarrollo.* 2011;29:186-201.
52. Bahabadi FN, Farpoor MH, Mehrizi MH. Removal of Cd, Cu and Zn ions from aqueous solutions using natural and Fe modified sepiolite, zeolite and palygorskite clay minerals. *Water Sci Technol.* 2017;75(2):340-9.
53. Teixeira CPDAB, Jardim WDF. Processos oxidativos avançados: conceitos teóricos. Campinas: Universidade Estadual de Campinas; 2004. (Caderno Temático; 3).
54. Rauf MA, Ashraf SS. Fundamental principles and application of heterogeneous photocatalytic degradation of dyes in solution. *Chem Eng J.* 2009;151(1-3):10-8.
55. Rauf MA, Meentani MA, Hisaindee S. An overview on the photocatalytic degradation of azo dyes in the presence of TiO₂ doped with selective transition metals. *Desalination.* 2011;276(1-3):13-27.
56. Greco E, Ciliberto E, Cirino AME, Capitani D, Di Tullio V. A new preparation of doped photocatalytic TiO₂ anatase nanoparticles: a preliminary study for the removal of pollutants in confined museum areas. *Appl Phys, A Mater Sci Process.* 2016;122:530.
57. Malato S, Fernández-Ibáñez P, Maldonado MI, Blanco J, Gernjak W. Decontamination and disinfection of water by solar photocatalysis: recent overview and trends. *Catal Today.* 2009;147(1):1-59.
58. Rezaei M, Habibi-Yangjeh A. Simple and large scale refluxing method for preparation of Ce-doped ZnO nanostructures as highly efficient photocatalyst. *Appl Surf Sci.* 2013;265:591-6.
59. Gaya UI, Abdullah AH. Heterogeneous photocatalytic degradation of organic contaminants over titanium dioxide: a review of

- fundamentals, progress and problems. *J Photochem Photobiol Photochem Rev.* 2008;9(1):1-12.
60. Akpan UG, Hameed BH. Parameters affecting the photocatalytic degradation of dyes using TiO₂-based photocatalysts: a review. *J Hazard Mater.* 2009;170(2-3):520-9.
 61. Kertész S, Cakl J, Jiráňková H. Submerged hollow fiber microfiltration as a part of hybrid photocatalytic process for dye wastewater treatment. *Desalination.* 2014;343:106-12.
 62. Haque MM, Muneer M. Photodegradation of norfloxacin in aqueous suspensions of titanium dioxide. *J Hazard Mater.* 2007;145(1-2):51-7.
 63. Kaur J, Debnath J. Autophagy at the crossroads of catabolism and anabolism. *Nat Rev Mol Cell Biol.* 2015;16(8):461-72.